A General Algorithm for Computing the Bidimensional Spectral Green's Dyad in Multilayered Complex Bianisotropic Media: The Equivalent Boundary Method

Francisco L. Mesa, Ricardo Marqués, and Manuel Horno, *Member, IEEE*

***Abstract*—A systematic method to obtain the bidimensional spectral dyadic Green's function (BSDGF) of stratified planar structures with arbitrary complex bianisotropic layers is developed. The method is based on the uniqueness and equivalence electromagnetic theorems. A first-order partial differential formulation for the electromagnetic field inside each layer is used. An explicit algorithm makes it possible to go from the single-layer formulas to the general *n*-layer matrix formulation. The perturbative nature of the method provides good numerical efficiency and straightforward determination of asymptotic behavior.**

I. Introduction

PLANAR layered structures have played a significant role in microwave technology. This role is increasing day by day thanks to the investigations of new configurations (including different geometries or anisotropic substrates) as well as to advances in material technology for monolitic microwave integrated circuits (MMIC's). The increasing capacity and complexity of these MMIC's require that the passive components be versatile [1]. Printed antenna problems involving stratified complex substrates have also been a matter of particular attention in recent years [2]. So, for design applications, it should be very interesting to contemplate the possibility of treating a very general planar system such as that shown in Fig. 1. This structure supports lossless and infinitesimally thick metallizations over several interfaces, and every layer can present dielectric and/or magnetic anisotropy including losses. The inclusion of very general anisotropic multilayered substrate is justified because of the intrinsic or extrinsic anisotropy of many of materials used as substrates. The intrinsic anisotropy relates to the anisotropic behavior of certain dielectric crystals (in the millimeter and microwave frequency range), and the extrinsic anisotropy is acquired when the optical activity is taken into account or when semiconductors as well as ferrites

Manuscript received July 27, 1990; revised April 19, 1991. This work was supported by the DGICYT, Spain (Proj. n. PB87-0798-CO3-01).

The authors are with the Department of Electronics and Electromagnetism, University of Sevilla, Avd. Reina Mercedes s/n, 41012 Sevilla, Spain.

IEEE Log Number 9101657.

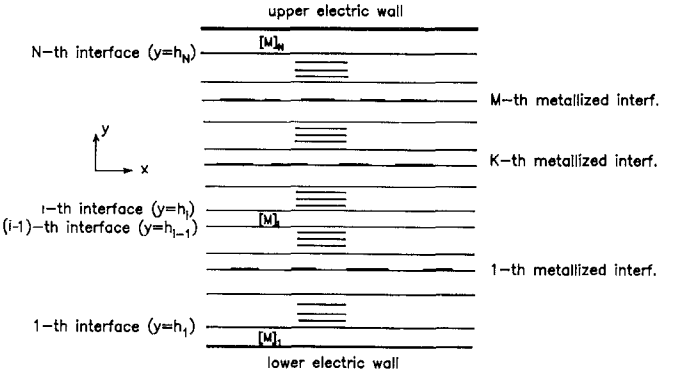

Fig. 1. Transverse section of the multilayered planar structure under study.

are biased by means of an external and static magnetic field. It is very well known that an arbitrary orientation of this biasing field makes all the elements of the dielectric permittivity or/and magnetic permeability distinct from zero.

The analysis of the electromagnetic field problem in the configuration depicted in Fig. 1 becomes simpler if the Fourier transformed domain (FTD)—or spectral domain—is used. This is mainly due to the fact that Green's function convolution integrals or series are turned into algebraic products. Moreover, the spectral dyadic Green's function (SDGF) and the bidimensional spectral dyadic Green's function (BSDGF) can be obtained following a straightforward systematic procedure, as will be shown in this work. If vectors $[\tilde{J}]$ and $[\tilde{E}]$ are assumed to be the (x,z) spectral components of the surface current and the electric field on every metallized interface, the $[\tilde{G}]$ matrix (i.e., BSDGF) will be here defined as $[\tilde{E}]=[\tilde{G}]\cdot[\tilde{J}]$ and the $[\tilde{L}]$ matrix (i.e., the inverse of the BSDGF) as $[\tilde{J}]=[\tilde{L}]\cdot[\tilde{E}]$. Once the BSDGF is determined, we can follow several methods (i.e., moment or iterative methods) to state the nondeterministic dispersion relation for transmission lines or the deterministic problem of the radiation pattern for antennas. The main purpose of this paper is to develop a general method (namely, the equivalent boundary method, EBM) to determine the BSDGF for

0018-9480/91/0900-1640$01.00

the general configuration of Fig. 1. The application of the BSDGF to the analysis of particular structures and its numerical treatment will be presented in future works. Nevertheless some results are presented now for purposes of comparison and in order to show the feasibility of the method.

A large number of works can be found in the literature dealing with the SDGF and BSDGF. We can highlight the transverse transmission line method (TTL), proposed in [3], in which an isotropic dielectric medium is analyzed based upon the decomposition of fields into transverse TE and TM modes. This method can be easily extended to all the configurations which provide for two decoupled equations relating current sources and fields: one for transverse TE fields and another for transverse TM fields. A uniaxial anisotropic dielectric with its optical axis perpendicular to the interfaces fulfills this condition [4]. The studies [5], [6], and [7] follow partly this TE and TM (or LSE and LSM) decomposition. This scheme is also followed in [8] to obtain the BSDGF when the distribution of electrical sources in the isotropic dielectric is tridimensional. It is necessary to use a different approach in order to analyze more general substrates such as uniaxial and biaxial dielectric layers of arbitrary orientation, magnetized ferrites and semiconductors, and bianisotropic media. Most methods dealing with these media are based upon the transverse propagation matrix scheme [9]–[11]. The method proposed in [9] has been found to be the most general because it makes it possible to study configurations with bianisotropic media. Nevertheless, there is no simple way to build up a general transverse propagation matrix algorithm to analyze general multilayered, multiconductor structures.

The equivalent boundary method (EBM), which is explained in this work, is a generalization of the method proposed by certain of the authors in [12] to obtain the SDGF. It is quite different from the TTL method and the propagation matrix method. The EBM is able to deal with any number of layers and any kind of linear substrate (from the simplest isotropic dielectric to more general bianisotropic lossy media). It will be shown that this method leads to a compact algorithm very suitable for programming. The algorithm also shows very stable numerical behavior.

The EBM is partly based on the equivalence and uniqueness theorems for electromagnetic fields [12]. One of the main features of the EBM is that its objective is to obtain not the BSDGF but its inverse. This provides two important consequences in relation to the electromagnetic theorems mentioned above. First, the inverse of the BSGDF will be a block tridiagonal matrix. This fact, together with its possible symmetry properties, can substantially reduce the computation time necessary to obtain this matrix when metallizations on several interfaces are involved. Second, it makes possible the reduction of the multilayer problem to a chain of much simpler problems of just one layer. (In the quasi-TEM case, a very similar approach can be used to determine the spectral Green's function [18]–[20].) Some works, such as [13]–[16], analyze this one-layer problem. In this work, a (4×4) matrix technique is used to solve the involved partial differential equations. This technique was proposed in [17] and adapted to the FTD in [9].

II. Bidimensional Spectral Dyadic Green's Function

In this section, we will develop a method to obtain the BSDGF for the general system depicted in Fig. 1. The $[\boldsymbol{L}]$ matrix will be expressed in terms of (2×2) matrices related to some single-layer problems which will be unambiguously formulated. Although the main features of this procedure were developed in [12] by some of the present authors, a brief exposition is necessary here for a good understanding of the method. The system depicted in Fig. 1 is composed by N bianisotropic layers with $N-1$ interfaces and upper and lower boundary electric walls. Every layer shows a linear constitutive relation between the $\boldsymbol{D}, \boldsymbol{B}$ and $\boldsymbol{E}, \boldsymbol{H}$ vectors, which will be characterized by the (6×6) $[M]_i$ matrix:

$$[M]_i = \begin{bmatrix} [\epsilon]_i & [\rho]_i \\ [\rho']_i & [\mu]_i \end{bmatrix}_i \quad (m_{ij} = m'_{ij} + jm''_{ij}). \tag{1}$$

This tensor is composed of four (3×3) tensors: the electric permittivity tensor $[\epsilon]_i$, the magnetic permeability tensor $[\mu]_i$, and the optical activity tensors $[\rho]_i$ and $[\rho']_i$. M of the $N-1$ interfaces show metallizations (references to any layer or interface will be denoted by lowercase subscripts and references to metallized interfaces will be denoted by uppercase subscripts). It should be noted that this structure is invariant when a translation is carried out in the $(x-z)$ plane. Thus, the spatial dyadic Green's function will show the following dependence with respect to variables x and z: $[\boldsymbol{G}(x, x', y, y', z, z')] = [\boldsymbol{G}(x - x', y, y', z - z')]$ and hence the convolution products involving this function are turned into algebraic products in the Fourier domain.

The uniqueness theorem for the electromagnetic field [21] tell us that the electric field at any point within a given boundary is completely known in terms of the electric field distribution on that boundary and the sources within it. Hence, in order to analyze the general configuration of Fig. 1, we now consider just a part of this, which is shown in Fig. 2. This is made because the above theorem allows us to substitute all the effects of the rest of the structure by knowing the electric field distribution on the external metallized interfaces. From the application of the uniqueness theorem to the configuration of Fig. 2 and the linear constitutive relations of the substrates, it follows that the electric field at any point between the $(K-1)$ and $(K+1)$ metallized interfaces is certainly determined in terms of the transverse electric fields at these interfaces, $\boldsymbol{E}_{t,K-1}$ and $\boldsymbol{E}_{t,K+1}$, and the free current sources on the metallized interface, $\boldsymbol{J}_K$.

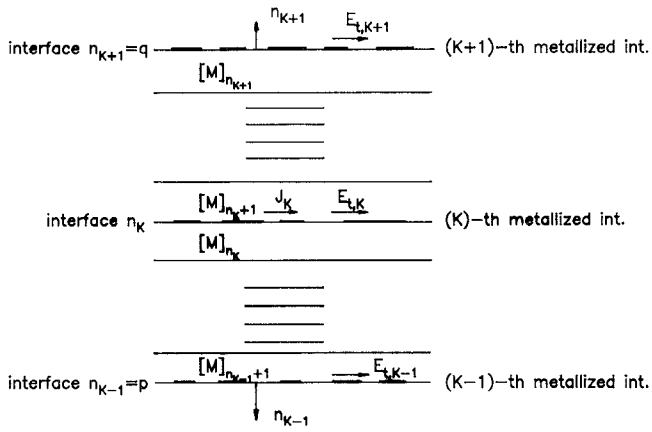

Fig. 2. Transverse partial view of Fig. 1 including just three metallized interfaces.

We can also make use of the equivalence theorem [21] to turn the electric boundary conditions at the $(K-1)$ and $(K+1)$ interfaces into other *equivalent boundary conditions*. These *equivalent boundary conditions* are set up by placing perfect conducting plates at the $(K-1)$ and $(K+1)$ interfaces and, on top of them, two sheets of fictitious *magnetic current* $\boldsymbol{M}_L = \boldsymbol{E}_{t,L} \times \boldsymbol{n}_L$ $(L = K-1, K+1)$ [21]. The relation between $\boldsymbol{E}_{t,K}$ and the sources $\boldsymbol{M}_L$ and $\boldsymbol{J}_K$ must show the form of a sum of convolution products [12] for linear media. If $\boldsymbol{M}_L$ is substituted in terms of $\boldsymbol{E}_{t,L}$, we arrive at the following expression:

$$\begin{aligned}\boldsymbol{E}_{t,K}(x,z,y) = &\int_{-\infty}^{\infty}\int_{-\infty}^{\infty} [\boldsymbol{F}(x-x',z-z',y)]_{K,K} \\ &\cdot \boldsymbol{J}_K(x',z',y)\,dx'\,dz' \\ &+ \int_{-\infty}^{\infty}\int_{-\infty}^{\infty} [\boldsymbol{D}(x-x',z-z',y)]_{K,K-1} \\ &\cdot \boldsymbol{E}_{t,K-1}(x',z',y)\,dx'\,dz' \\ &+ \int_{-\infty}^{\infty}\int_{-\infty}^{\infty} [\boldsymbol{D}(x-x',z-z',y)]_{K,K+1} \\ &\cdot \boldsymbol{E}_{t,K+1}(x',z',y)\,dx'\,dz' \end{aligned} \quad (2)$$

where $[\boldsymbol{F}]_{K,K}$, $[\boldsymbol{D}]_{K,K-1}$, and $[\boldsymbol{D}]_{K,K+1}$ are dyads which depend only on the dimensions and characteristics of the structure. Note that in (2), all the sources above the $(K+1)$ interface and below the $(K-1)$ interface have been replaced by *equivalent* fields ($E_{t,K+1}$ and $E_{t,K-1}$) at these interfaces. The systematic application of this property of the electromagnetic field in linear media constitutes the essence of the EBM.

The above expression suggests the use of the FTD in order to achieve an algebraic expression. The two-dimensional Fourier transform, i.e.,

$$\tilde{f}(k_x,k_z,y) = \int_{-\infty}^{\infty}\int_{-\infty}^{\infty} f(x,z,y)\,e^{j(k_x+k_z)}\,dx\,dz \quad (3)$$

applied to the electromagnetic fields can be interpreted as the decomposition of these fields into propagating fields with a transverse propagation vector $\boldsymbol{k}_t = (k_x, k_z)^T$ (the superscript T denoting transpose). If expression (2) is translated to the FTD via (3) and some algebraic manipulations are carried out on the resulting algebraic vector equation, we will be able to write the following expression for the FTD free current source vector on the Kth metallized interface:

$$\begin{aligned}\tilde{\boldsymbol{J}}_K(k_x,k_z,y) = &[\boldsymbol{L}(k_x,k_z,y)]_{K,K-1}\cdot\tilde{\boldsymbol{E}}_{t,K-1}(k_x,k_z,y) \\ &+ [\boldsymbol{L}(k_x,k_z,y)]_{K,K}\cdot\tilde{\boldsymbol{E}}_{t,K}(k_x,k_z,y) \\ &+ [\boldsymbol{L}(k_x,k_z,y)]_{K,K+1}\cdot\tilde{\boldsymbol{E}}_{t,K+1}(k_x,k_z,y)\end{aligned} \quad (4)$$

$[\boldsymbol{L}]_{I,J}$ $(I = K, J = K-1, K, K+1)$ being (2×2) matrices. The effect of the rest of the electric fields is taken into account by means of the other relations analogous to (4) with $K = 1$ to M.

The above expression holds a physical interpretation for the $[\boldsymbol{L}]_{I,J}$ matrices since these matrices relate the transverse free current source $\tilde{\boldsymbol{J}}_I$ on the Ith interface to the transverse electric field $\tilde{\boldsymbol{E}}_J$ on the Jth interface when the other two interfaces are assumed to be electric walls. This fact is depicted in Fig. 3.

If we now express relation (4) over all the metallized interfaces, we arrive at

$$\begin{bmatrix}\tilde{\boldsymbol{J}}_1\\ \tilde{\boldsymbol{J}}_2\\ \tilde{\boldsymbol{J}}_3\\ \tilde{\boldsymbol{J}}_4\\ \vdots\\ \tilde{\boldsymbol{J}}_M\end{bmatrix} = \begin{bmatrix}[\boldsymbol{L}]_{11} & [\boldsymbol{L}]_{12} & [0] & [0] & \cdots & [0]\\ [\boldsymbol{L}]_{21} & [\boldsymbol{L}]_{22} & [\boldsymbol{L}]_{23} & [0] & \cdots & [0]\\ [0] & [\boldsymbol{L}]_{32} & [\boldsymbol{L}]_{33} & [\boldsymbol{L}]_{34} & \cdots & [0]\\ [0] & [0] & [\boldsymbol{L}]_{43} & [\boldsymbol{L}]_{44} & \cdots & [0]\\ \vdots & \vdots & \vdots & \vdots & \ddots & \vdots\\ [0] & [0] & [0] & [0] & \cdots & [\boldsymbol{L}]_{MM}\end{bmatrix}\begin{bmatrix}\tilde{\boldsymbol{E}}_{t,1}\\ \tilde{\boldsymbol{E}}_{t,2}\\ \tilde{\boldsymbol{E}}_{t,3}\\ \tilde{\boldsymbol{E}}_{t,4}\\ \vdots\\ \tilde{\boldsymbol{E}}_{t,M}\end{bmatrix} \quad (5)$$

Note the block tridiagonal nature of the $[\boldsymbol{L}]$ $(2M\times2M)$ matrix.

Equations (4) and (5) do not show a direct coupling between $(\tilde{\boldsymbol{J}}_K)$ and $(\tilde{\boldsymbol{E}}_L)$ for $|L-K|>1$. Therefore, changes in the field at the $(K+2)$ interface, for example,

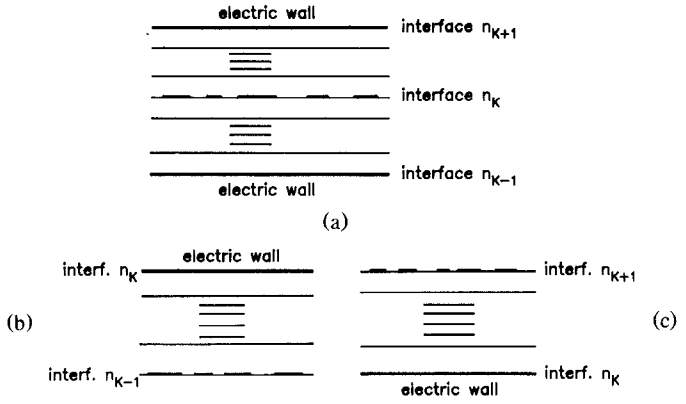

Fig. 3. Configurations associated with (a) $[L]_{K,K}$, (b) $[L]_{K,K-1}$, and (c) $[L]_{K,K+1}$.

do not have any effect on $(\tilde{J}_K)$, provided that $(\tilde{E}_{K+1})$ remains constant, i.e., provided that $(\tilde{J}_{K+1})$ changes in the exact amount to leave $(\tilde{E}_{t,K+1})$ unchanged. This is not a surprising fact since it is always possible to introduce a current density $(\tilde{J}_{K+1})$ at the $(K+1)$ interface to hold the field $(\tilde{E}_{t,K+1})$ unchanged at this interface, regardless of the fields and sources above that interface (equivalence theorem, [21]).

If we are dealing just with slotlike structures, the required matrix is directly the $[L]$ matrix. When other types of structures are analyzed, $[G]$ being the required matrix now, it will be necessary to invert the $[L]$ matrix. Nevertheless, on the one hand there are efficient computing methods to invert tridiagonal matrices; on the other, the computation of the $[L]_{I,J}$ matrices involves only calculus concerning a minor number of layers (see Fig. 3) than the original structure.

It should be noted that closed structures with rectangular boundary conditions could also be treated by using the FTD techniques (together with the BSDGF shown in (5)) if this closed structure could be viewed as one period of a bidimensional or tridimensional periodic configuration. Fourier integral transforms should be also converted into Fourier series transforms adapted to the new lateral boundary conditions in the problem.

This treatment is possible in boxed structures if lateral metallic sidewalls are perpendicular either to a main axis of anisotropy, for intrinsic anisotropic dielectric layers, or to the external biasing magnetization field, for gyrotropic layers. Nevertheless, from a practical standpoint, all kinds of layered boxed structures can be analyzed by using FTD techniques if the sidewall effects are assumed to be neglected.

From (5), we can see that the zeros (k_x, k_z) of the determinant of the $[L]$ matrix are associated with the transverse propagation vectors of the different propagation modes in the whole structure in Fig. 1, without metallizations at the internal interfaces. In the same way, the poles of this determinant are associated with any of the propagating modes at any of the substructures formed when the metallized interfaces are whole electric walls. Propagation vectors in suitable boxed structures form a

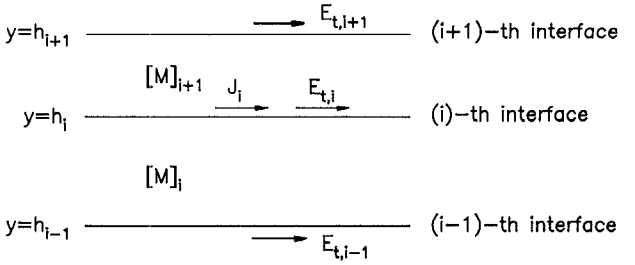

Fig. 4. Two-layer configuration.

discrete subset of the continuous bidimensional spectrum associated with the corresponding open structure.

A. Computation of $[L]_{I,J}$

As mentioned in the previous section, the computation of the $[L]_{I,J}$ matrices is related to the analysis of the configurations drawn in Fig. 3. These structures will be the subject of this subsection. If we now follow an analogous procedure for one of these configurations, as was followed with the previous general system, this will lead to the relevant fact that our current problem can be formulated by means of some new (2×2) $[g]_{i,j}$ matrices which will be associated with problems of just one and two layers. The analysis of the configurations of Fig. 3, when the mentioned procedure is carried out [12], is therefore reduced to the analysis of the simpler two-layer structure depicted in Fig. 4. The following identity, similar to (4), is obtained:

$$\tilde{J}_i = [g]_{i,i-1}\cdot\tilde{E}_{t,i-1} + [g]_{i,i}\cdot\tilde{E}_{t,i} + [g]_{i,i+1}\cdot\tilde{E}_{t,i+1}. \quad (6)$$

Equation (6) relates the possible free current sources $\tilde{J}_i$ at the ith interface to the transverse electric fields at that interface and the adjacent ones. We can associate a physical significance to these $[g]_{i,j}$ $(j=i-1,i,i+1)$ in a similar way to that carried out in the preceding section for the $[L]_{I,J}$ matrices. By doing this, the problem of the general system will have been essentially simplified. This fact will make it possible to deal with the general system regardless of the number and distribution of layers and metallizations. The computation of the $[g]_{i,j}$ matrices will be the aim of the next section.

In order to compute the $[L]_{I,J}$, assuming that the $[g]_{i,j}$ have been obtained, we will have to carry out a tedious but straightforward procedure. This procedure is developed by using (6) to eliminate the transverse electric field at the ith interface when this interface is not metallized, i.e., $\tilde{J}_i = 0$. After some algebraic manipulations, the following identity is obtained:

$$[L]_{K,K} = [A]_K^{n'_K} + [B]_K^{n'_K} - [g]_{n_K,n_K} \quad (7)$$

$$[L]_{K,K-1} = [C]_K^{n'_K} \quad (8)$$

$$[L]_{K,K+1} = [D]_K^{n'_K} \quad (9)$$

n_K being the number of layers underneath the Kth interface, $n'_K = n_K - n_{K-1}$, and $n''_K = n_{K+1} - n_K$. The above identity is built up by means of the following recurrence

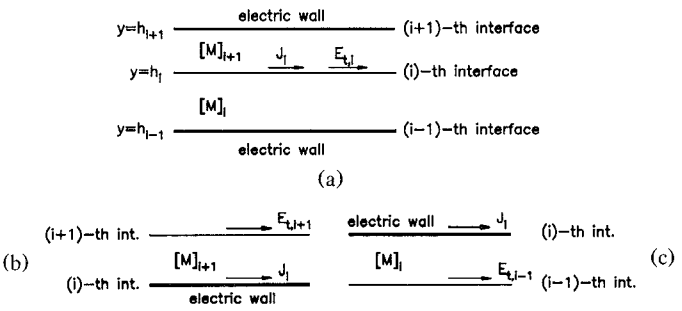

Fig. 5. (a) Two-layer configuration associated with $[g]_{i,i}$. Single-layer configurations associated with (b) $[g]_{i,i+1}$ and (c) $[g]_{i,i-1}$. In (b) and (c), J_i is the surface free current source in the conductors.

algorithm:

$$[A]_K^1 = [g]_{p+1,p+1} \tag{10}$$

$$[B]_K^1 = [g]_{q-1,q-1} \tag{11}$$

$$[C]_K^1 = [g]_{p+1,p} \tag{12}$$

$$[D]_K^1 = [g]_{q-1,q} \tag{13}$$

$$[A]_K^j = [g]_{p+j,p+j} - [g]_{p+j,p+j-1} \cdot \left([A]_K^{j-1}\right)^{-1} \cdot [g]_{p+j-1,p+j} \tag{14}$$

$$[B]_K^i = [g]_{q-i,q-i} - [g]_{q-i,q-i+1} \cdot \left([B]_K^{i-1}\right)^{-1} \cdot [g]_{q-i+1,q-i} \tag{15}$$

$$[C]_K^j = -[g]_{p+j,p+j-1} \cdot \left([A]_K^{j-1}\right)^{-1} \cdot [C]_K^{j-1} \tag{16}$$

$$[D]_K^i = -[g]_{q-i,q-i+1} \cdot \left([B]_K^{i-1}\right)^{-1} \cdot [D]_K^{i-1} \tag{17}$$

with $p = n_{K-1}$, $q = n_{K+1}$, $j = 2, \cdots, n'_K$, and $i = 2, \cdots, n''_K$. Note that all the above expressions are made up by means of algebraic operations of the (2×2) $[g]_{i,j}$ matrices. We can now build the tridiagonal block matrix $[L]$ of (5) once all the $[L]_{I,J}$ matrices are obtained.

B. Reduction to single-layer problem

The computation of the (2×2) $[g]_{i,j}$ matrices is better understood if each matrix can be interpreted as

$$\tilde{J}_i = [g]_{i,i-1} \cdot \tilde{E}_{t,i-1}\big|_{\tilde{E}_{t,i}=0} \tag{18}$$

$$\tilde{J}_i = [g]_{i,i} \cdot \tilde{E}_{t,i}\big|_{\tilde{E}_{t,i-1}=\tilde{E}_{t,i+1}=0} \tag{19}$$

$$\tilde{J}_i = [g]_{i,i+1} \cdot \tilde{E}_{t,i+1}\big|_{\tilde{E}_{t,i}=0}. \tag{20}$$

Following (18)–(20) we can explicitly depict the structure associated with each $[g]_{i,j}$ matrix. It can be seen in Fig. 5 that we now have, on the one hand, two problems of one layer with one electric wall and, on the other hand, one problem of two layers with two electric walls. However, the two-layer problem can be decomposed into two problems of one layer and one electric wall, as suggested by the application of the boundary conditions at the ith interface. So, we can express the free current source at the ith interface by means of

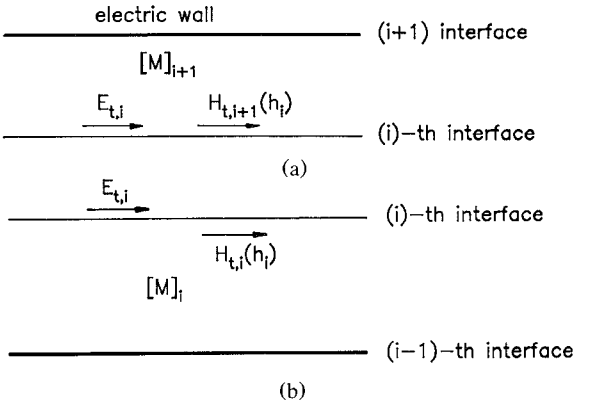

Fig. 6. Single-layer configurations associated with (a) $[g^+]_{i,i}$ and (b) $[g^-]_{i,i}$.

$$\tilde{J}_i = [T] \cdot \left(\tilde{H}_{t,i+1}(h_i) - \tilde{H}_{t,i}(h_i)\right) \tag{21}$$

with $[T] = \begin{pmatrix} 0 & 1 \\ -1 & 0 \end{pmatrix}$. We can therefore decompose the $[g]_{i,i}$ matrix into two matrices associated with the single-layer problem (see Fig. 6) in such a way that

$$[g]_{i,i} = [g^+]_{i,i} + [g^-]_{i,i}. \tag{22}$$

These matrices can be interpreted as follows:

$$\tilde{H}_{t,i-1}(h_i) = [T]^{-1} \cdot \left([g^+]_{i,i} \cdot \tilde{E}_{t,i}\right)\big|_{\tilde{E}_{t,i+1}=0} \tag{23}$$

$$\tilde{H}_{t,i}(h_i) = [T]^{-1} \cdot \left([g^-]_{i,i} \cdot \tilde{E}_{t,i}\right)\big|_{\tilde{E}_{t,i-1}=0}. \tag{24}$$

From (23) and (24), we can see that these $[g^+]_{i,i}$ and $[g^-]_{i,i}$ matrices are actually the admittance matrices relating the transverse electric to the magnetic fields at the ith interface in the structures shown in, respectively, parts (a) and (b) of Fig. 6.

III. Analysis of $[g]_{i,j}$ Matrices

In this section the computational method for obtaining the $[g]_{i,j}$ matrices of the preceding section will be developed. We will also analyze the properties of these elementary matrices for the more common cases, in which the layer is either reciprocal or lossless. Some considerations will be finally made on the main numerical features of the method proposed here.

A. Computation of $[g]_{i,j}$ Matrices

At this point, it is obvious that all the problems have been reduced to find the relations between the transverse electric and magnetic fields in a configuration with just one complex bianisotropic layer. In order to solve it, we will follow a (4×4) matrix scheme similar to that adapted to the FTD in [9]. When a time harmonic dependence $\exp(j\omega t)$ of the fields is assumed, we can write the

second and fourth Maxwell's equations for the ith layer as

$$\begin{bmatrix} [\mathscr{R}] & [0] \\ [0] & [\mathscr{R}] \end{bmatrix}_{(6\times 6)} \cdot \begin{bmatrix} \tilde{E}_i \\ \tilde{H}_i \end{bmatrix} = j\omega \begin{bmatrix} -[\rho']_i & -[\mu]_i \\ [\epsilon]_i & [\rho]_i \end{bmatrix}_{(6\times 6)} \cdot \begin{bmatrix} \tilde{E}_i \\ \tilde{H}_i \end{bmatrix} \quad (25)$$

with

$$[\mathscr{R}]_{(3\times 3)} = \begin{bmatrix} 0 & jk_z & \dfrac{\partial}{\partial y} \\ -jk_z & 0 & jk_x \\ -\dfrac{\partial}{\partial y} & -jk_x & 0 \end{bmatrix}$$

$$\tilde{E}_i = \begin{bmatrix} \tilde{E}_{x,i}(k_x, k_z, y) \\ \tilde{E}_{y,i}(k_x, k_z, y) \\ \tilde{E}_{z,i}(k_x, k_z, y) \end{bmatrix}$$

and

$$\tilde{H}_i = \begin{bmatrix} \tilde{H}_{x,i}(k_x, k_z, y) \\ \tilde{H}_{y,i}(k_x, k_z, y) \\ \tilde{H}_{z,i}(k_x, k_z, y) \end{bmatrix}.$$

We can eliminate the y components of the $\tilde{E}_i, \tilde{H}_i$ fields by operating in the second and fifth rows of (25) on account of the algebraic nature of these rows. Once this has been carried out, the following first-order matrix equation of rank 4 is obtained:

$$\left\{ [U] \frac{\partial}{\partial y} - j\omega [Q]_i \right\} X_i = 0 \quad (26)$$

with $[U]$ being the (4×4) unity matrix, $[Q]_i$ the (4×4) matrix resulting from all the algebraic manipulations, and $X_i = [\tilde{E}_{x,i} \tilde{E}_{z,i} \tilde{H}_{x,i} \tilde{H}_{z,i}]^T$. All the elements of the $[Q]_i$ matrix are shown in the Appendix for the common case of dielectric and magnetic anisotropy. In [9] an analogous matrix is shown for the general case. The solution of (26) is a vector which can be written as

$$X_i(y) = \exp(j\omega [Q]_i y) \cdot X_{o,i} \quad (27)$$

where $X_{o,i}$ is a constant vector to be determined according to the boundary conditions and $\exp(j\omega[Q]_i y)$ is a (4×4) matrix which can be related to the eigenvalues and eigenvectors of $[Q]_i$ by means of the Cayley–Hamilton theorem. As can be noted from (27), we can express the electromagnetic field at any y plane in terms of the field at another y' plane. Thus, we can write at the $(i+1)$ layer that

$$X_{i+1}(h_{i+1}) = \exp(j\omega [Q]_{i+1}(h_{i+1} - h_i)) \cdot X_{i+1}(h_i) = [P]_{i+1} \cdot X_{i+1}(h_i) \quad (28)$$

and from the properties of the exponential matrix that $X_{i+1}(h_i) = [R]_{i+1} \cdot X_{i+1}(h_{i+1})$, with $[R]_{i+1} = [P]_{i+1}^{-1}$. We now have to take into account the boundary conditions for the single-layer configurations of Fig. 5(b) and (c) and Fig. 6(a) and (b) in order to determine the relation between currents and fields. In case we are interested in computing $[g^+]_{i,i}$, (28) can be rewritten as

$$\begin{bmatrix} \tilde{E}_{t,i+1}(h_{i+1}) \\ \tilde{H}_{t,i+1}(h_{i+1}) \end{bmatrix} = \begin{bmatrix} [P_{11}]_{i+1} & [P_{12}]_{i+1} \\ [P_{21}]_{i+1} & [P_{22}]_{i+1} \end{bmatrix} \cdot \begin{bmatrix} \tilde{E}_{t,i+1}(h_i) \\ \tilde{H}_{t,i+1}(h_i) \end{bmatrix} \quad (29)$$

where $[P_{i,j}]_{i+1}$ denotes one of the four (2×2) matrices in which the (4×4) $[P]_{i+1}$ matrix is split. Since $\tilde{E}_{t,i+1}(h_{i+1}) = 0$ (see Fig. 6(a)), we obtain

$$\tilde{H}_{t,i+1}(h_i) = -\left\{ ([P_{12}]_{i+1})^{-1} \cdot [P_{11}]_{i+1} \right\} \cdot \tilde{E}_{t,i+1}(h_i) \quad (30)$$

and following (22) and (23), $[g^+]_{i,i}$ is already determined. If the necessary operations are carried out for the other single-layer configurations, we reach

$$[g^-]_{i,i} = [T] \cdot \left[([R_{12}]_i)^{-1} \cdot [R_{11}]_i \right] \quad (31)$$

$$[g^+]_{i,i} = -[T] \cdot \left[([P_{12}]_{i+1})^{-1} \cdot [P_{11}]_{i+1} \right] \quad (32)$$

$$[g]_{i,i+1} = [T] \cdot ([P_{12}]_{i+1})^{-1} \quad (33)$$

$$[g]_{i,i-1} = -[T] \cdot ([R_{12}]_i)^{-1}. \quad (34)$$

Once these matrices are obtained, we can easily follow the algorithms shown in (7)–(17) in order to build up the inverse or the BSDGF.

B. Properties of $[g]_{i,j}$ Matrices

Since the complex general problem has been formulated in terms of several simpler single-layer problems, we can now take into account the symmetry properties of the characteristic tensor of each layer to state the properties of the (2×2) corresponding $[g]_{i,j}$ matrices. We will show these properties when the involved layers are assumed to be reciprocal or lossless. For example, in order to find the properties of the $[g]_{i,i-1}$ and $[g]_{i-1,i}$ matrices, we will first analyze an N-layer configuration similar to that depicted in Fig. 1. But we now consider that this configuration does not show internal metallized interfaces and the ith layer is assumed to be reciprocal [22], i.e., $[\epsilon]_i = [\epsilon]_i^T$, $[\mu]_i = [\mu]_i^T$, and $[\rho']_i = -[\rho]_i^T$. This case includes the common intrinsic electric and/or magnetic anisotropy but not gyrotropic effects. The reciprocity theorem [22] for such a configuration can be written for two different free current sources and electric fields inside the ith layer as

$$\iint_{S_i} [H_i'(r) \times E_i(r) - H_i(r) \times E_i'(r)] \, dS_i + \iint_{S_{i-1}} [H_i'(r) \times E_i(r) - H_i(r) \times E_i'(r)] \, dS_{i-1} = \int_\Omega [E(r) \cdot J'(r) - E'(r) \cdot J(r)] \, dV \quad (35)$$

with the surface integrals extended over the ith and $(i-1)$ interfaces limiting the ith layer and the volume integral extended over the whole ith layer. We now choose the same current and electric field of Fig. 5(c) for $\boldsymbol{J}(\boldsymbol{r})$ and $\boldsymbol{E}(\boldsymbol{r})$ and the current and electric field of Fig. 5(b) for the case where the $(i+1)$ layer is replaced by the ith layer for $\boldsymbol{J}'(\boldsymbol{r})$ and $\boldsymbol{E}'(\boldsymbol{r})$. Taking into account the boundary conditions imposed by the electric walls ($\boldsymbol{E}_t(y=h_t)=0$; $\tilde{\boldsymbol{E}}'_t(y=h_{t-1})=0$), expression (35) becomes

$$\int\int_{S_t} \boldsymbol{E}_{t,t}(\boldsymbol{r})\cdot\boldsymbol{J}'_t(\boldsymbol{r})\,dS_t = \int\int_{S_{t-1}} \boldsymbol{E}'_{t,t-1}(\boldsymbol{r})\cdot\boldsymbol{J}_{t-1}(\boldsymbol{r})\,dS_{t-1} \tag{36}$$

with the integrals extended to all the points at the ith and $(i-1)$ interfaces. If the following identity is considered

$$\{\tilde{f}(-k_x,-k_z,y)\}^* = \mathcal{F}\{f^*(x,z,y)\} \tag{37}$$

(f^* denoting conjugate complex of f and $\mathcal{F}$ the Fourier transform), once Parseval's theorem is applied to (36), we obtain

$$\begin{aligned}\int_{-\infty}^{\infty}\int_{-\infty}^{\infty} &\tilde{\boldsymbol{E}}_{t,i}(k_x,k_z,y)\cdot\tilde{\boldsymbol{J}}'_i(-k_x,-k_z,y)\,dk_x\,dk_z \\ &= \int_{-\infty}^{\infty}\int_{-\infty}^{\infty} \tilde{\boldsymbol{E}}'_{t,i-1}(k_x,k_z,y) \\ &\quad\cdot\tilde{\boldsymbol{J}}_{i-1}(-k_x,-k_z,y)\,dk_x\,dk_z.\end{aligned} \tag{38}$$

If the free current sources are now expressed in terms of the electric field by means of the previously defined matrices (eqs. (18)–(20) and (22)), we will rewrite (38) as

$$\begin{aligned}\int_{-\infty}^{\infty}\int_{-\infty}^{\infty} &\tilde{\boldsymbol{E}}_t(k_x,k_z,y)\cdot\left[[\boldsymbol{g}(-k_x,-k_z,y)]_{i,t-1}\right. \\ &\left.\cdot\tilde{\boldsymbol{E}}_{t,t-1}(-k_x,-k_z,y)\right]dk_x\,dk_z \\ &= \int_{-\infty}^{\infty}\int_{-\infty}^{\infty} \tilde{\boldsymbol{E}}_{t,i-1}(k_x,k_z,y)\cdot\left[[\boldsymbol{g}(-k_x,-k_z,y)]_{t-1,t}\right. \\ &\left.\cdot\tilde{\boldsymbol{E}}_{t,i}(-k_x,-k_z,y)\right]dk_x\,dk_z \\ &= \int_{-\infty}^{\infty}\int_{-\infty}^{\infty} \tilde{\boldsymbol{E}}_{t,t-1}(-k_x,-k_z,y)\cdot\left[[\boldsymbol{g}(k_x,k_z,y)]_{i-1,t}\right. \\ &\left.\cdot\tilde{\boldsymbol{E}}_{t,t}(k_x,k_z,y)\right]dk_x\,dk_z.\end{aligned} \tag{39}$$

The above identity yields that $[\boldsymbol{g}(-k_x,-k_z,y)]_{i-1,i} = [\boldsymbol{g}(k_x,k_z,y)]^T_{i,t-1}$.

When the characteristic tensor $[\boldsymbol{M}_t]$ is assumed to be Hermitian, i.e., for lossless layers, the reciprocity theorem is not (35) but it is given in [23]. We can follow an analogous procedure to state the properties of any other matrices related to the single-layer configurations (any of these matrices will be generically denote by $[\boldsymbol{p}]_{t,j}$, $(j=i-1,i,i+1)$). If this is carried out, we will find that

$$[\boldsymbol{p}(k_x,k_z,y)]_{t,j} = \begin{cases} [\boldsymbol{p}(-k_x,-k_z,y)]^T_{j,t} & \text{if the involved medium is reciprocal} \\ -[\boldsymbol{p}(k_x,k_z,y)]^\dagger_{j,i} & \text{if the involved medium is lossless.}\end{cases} \tag{40}$$

These properties are easily transposed to the $[\boldsymbol{L}]_{I,J}$ and BSDGF matrices when the substrates involved in the computation of these matrices show the same properties. The symmetries provided by these properties can significantly reduce the necessary work to compute the BSDGF. It can also be very useful in applications of the BSDGF which imply numerical integrations.

IV. Results

A. Theoretical and Numerical Considerations

We are now interested in obtaining $[\boldsymbol{g}]_{t,j}$ matrices in the simplest case, i.e., the isotropic dielectric layered configuration. If the present procedure is followed, the first step to take is the calculus of the exponential matrix $\exp(j\omega[\boldsymbol{Q}]_{t+1}y)$. It can be observed in the Appendix for this simple case that

$$[\boldsymbol{P}]_{i+1}(y) = \exp\left(j\omega[\boldsymbol{Q}]_{t+1}y\right),$$

with

$$[\boldsymbol{Q}]_{i+1} = \begin{bmatrix} [0] & [\boldsymbol{Q}_{12}]_{i+1} \\ [\boldsymbol{Q}_{21}]_{i+1} & [0]\end{bmatrix}_{(4\times4)}. \tag{41}$$

The presence of these two zero submatrices in $[\boldsymbol{Q}]_{i+1}$ makes it very easy to obtain the exponential matrix:

$$[\boldsymbol{P}]_{t+1}(y) = \begin{bmatrix} [U]\cosh(\Omega_{t+1}y) & \dfrac{j}{\Omega_{t+1}}[\boldsymbol{M}]_{t+1}\sinh(\Omega_{i+1}y) \\ \dfrac{\Omega_{t+1}}{j}[\boldsymbol{M}]^{-1}_{t+1}\sinh(\Omega_{t+1}y) & [U]\cosh(\Omega_{t+1}y)\end{bmatrix}$$

with

$$[\boldsymbol{M}]_{i+1}(y) = \begin{bmatrix} -\dfrac{k_xk_z}{\omega\epsilon_{i+1}} & \dfrac{k_x^2}{\omega\epsilon_{i+1}} - \omega\mu_{i+1} \\ -\dfrac{k_z^2}{\omega\epsilon_{i+1}} + \omega\mu_{i+1} & \dfrac{k_xk_z}{\omega\epsilon_{t+1}}\end{bmatrix}$$

and

$$\Omega_{i+1} = \sqrt{k_x^2+k_z^2-\omega^2\mu_{t+1}\epsilon_{t+1}}\,.$$

If we now follow expressions (31) and (33), it is found that

$$[g^+]_{i,i} = \frac{1}{j\omega\mu_{i+1}} \cdot \begin{bmatrix} -k_z^2 + \omega^2\mu_{i+1}\epsilon_{i+1} & k_x k_z \\ k_x k_z & k_x^2 - \omega^2\mu_{i+1}\epsilon_{i+1} \end{bmatrix} \cdot \frac{1}{\Omega_{i+1}} \coth\left[\Omega_{i+1}(h_{i+1} - h_i)\right] \quad (42)$$

$$[g]_{i,i+1} = -\frac{1}{j\omega\mu_{i+1}} \cdot \begin{bmatrix} -k_z^2 + \omega^2\mu_{i+1}\epsilon_{i+1} & k_x k_z \\ k_x k_z & k_x^2 - \omega^2\mu_{i+1}\epsilon_{i+1} \end{bmatrix} \cdot \frac{1}{\Omega_{i+1}} \operatorname{csch}\left[\Omega_{i+1}(h_{i+1} - h_i)\right] \quad (43)$$

these results being the same as those obtained in [16] for the isotropic case.

It can be seen in the above expressions that the functional dependence of the $[g]_{i,j}$ matrices in this simple case and for certain other intrinsic anisotropic dielectric layered configurations, as in [16], is mainly of the type $[g^{+,-}]_{i,i} \sim [K^{+,-}]\coth\{[K^{+,-}]\}$ and $[g]_{i,j} \sim [K]\operatorname{csch}\{[K]\}$ $(j \neq i)$. The (2×2) $[K^{+,-}]$ and $[K]$ matrices depend on the constitutive constant of the layer and show an algebraic dependence of the k_x and k_z in such a way that, for large k_x and k_z, $[g^{+,-}]_{i,i} \sim [K^{+,-}]$ and $[g]_{i,j} \sim [0]$ $(j \neq i)$. Similar behavior has been verified for the same matrices in the more involved structures treated in this work for large k_x and k_z.

From a detailed observation of (7)–(17), it can be said that the procedure to obtain the $[L]_{I,J}$ matrices is essentially a perturbative one. We can note, for example in (7), that the $[L]_{K,K}$ matrix shows a first-order dependence with the $[g]_{n_K,n_K}$ matrix, namely the effect of the adjacent layers to the metallized Kth interface, and a dependence of upper orders from the effect of the other layers. Thus, the $[L]_{I,J}$ matrices show essentially the same type of dependence implicit in the $[g]_{i,j}$ matrices for large k_x and k_z. This latter fact together with the perturbative feature of the mentioned matrices will make the numerical behavior of the EBM well conditioned. This behavior also avoids any numerical problems related to the increasing number of layers.

On the other hand, we will also be able to predict the asymptotic behaviour of the $[L]_{I,J}$ matrices on account of its perturbative nature. So, we can say that $[L]_{K,K} \sim [g]_{n_K,n_K}$ and $[L]_{K,L} \sim 0$. This asymptotic behavior can be very useful when numerical integration involving elements of the BSDGF is necessary.

B. Numerical Results

Some numerical data have been generated to show the numerical efficiency of the present algorithm. As mentioned above, the poles of the BSDGF stand for the propagation characteristics of the different modes in a multilayered planar guide without internal metallizations. This fact has been taken into account to analyze the two different guides, which are partially filled with ferrite and are shown in Figs. 7 and 8 respectively. Two orientations of the magnetizing field, H_o, have been considered, showing the data obtained to be in good agreement with the previous theoretical data [24, fig. 2(a)], [25, figs. 2 and 3] in both graphs. The dimensions and characteristics for

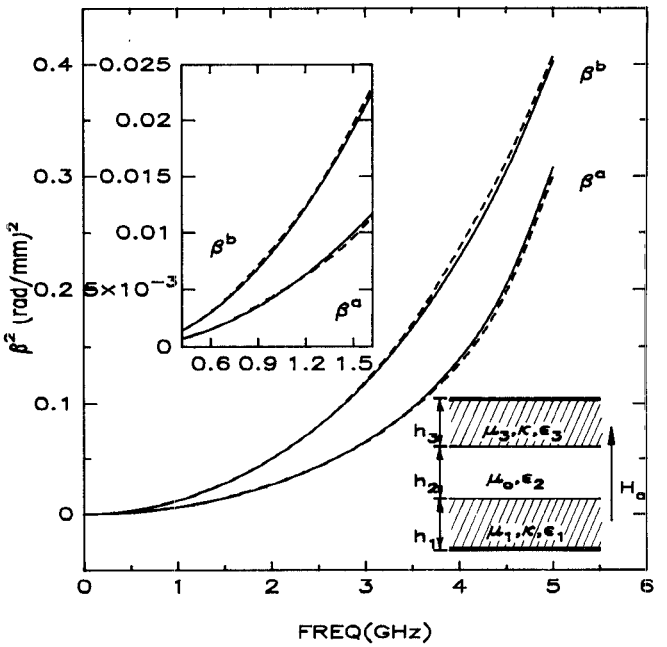

Fig. 7. Propagation constant for an asymmetrical ferrite–dielectric–ferrite parallel-plate line with $M_{s1} = 167.11$ kA/m, $M_{s3} = 139.26$ kA/m, $H_o = 159.24$ kA/m, $\epsilon_1 = 13.5$, $\epsilon_2 = 2.6$, $\epsilon_3 = 16$, $h_1 = 1.5$ mm. (β^a for $h_2 = 1$ mm, $h_3 = 3$ mm; β^b for $h_2 = 0$ mm, $h_3 = 4$ mm) (- - - - - -) [24, fig. 2(a)]; (———) our results.

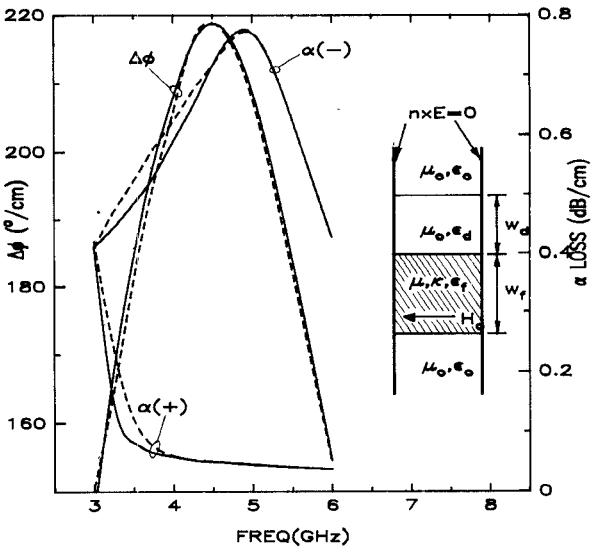

Fig. 8. Differential phase shift and insertion losses for the drawn guide with $4\pi M_s = 1780$ G, $H_o = 200$ Oe, $\Delta H_o = 45$ Oe, $\epsilon_f = 15$, $\epsilon_d = 96$, $w_d = w_f = 2$ mm. (- - - - - -) [25, figs. 2 and 3]; (———) our results.

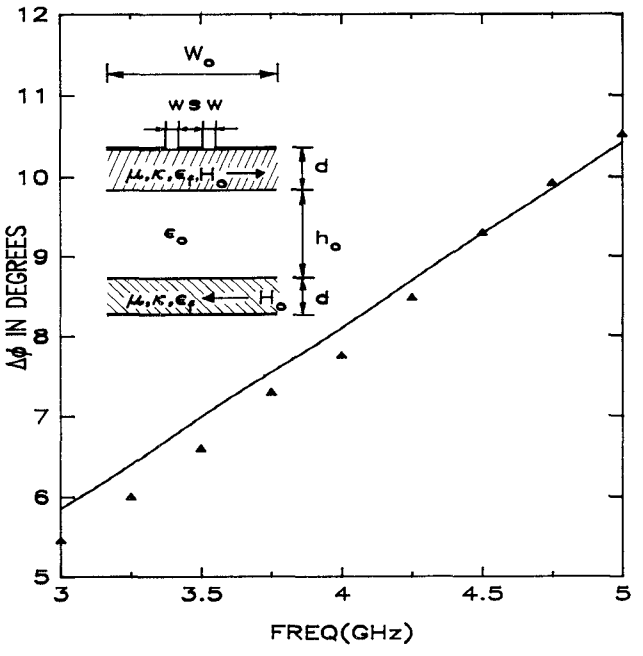

Fig. 9. Differential phase shift of a coplanar waveguide with $4\pi M_s = 493$ G, $H_o = 0$ Oe, $\epsilon_f = 14.8$, $d = 1.59$ mm, $h_o = 3.92$ mm, $w = 1$ mm, $s = 1.6$ mm, $W_o \mapsto \infty$ (▲ ▲ ▲ ▲) [10, fig. 10]; (———) our results.

both guides are detailed in the works cited. The CPU time required to compute the BSGDF for a given value of (k_x, k_z) was about 5 ms on a CONVEX-220 computer. If for instance the Muller method for searching complex zeros is employed, the total CPU time to obtain one datum from Figs. 7 and 8 was typically 60 ms.

In addition, the algorithm treated here has been combined with the Galerkin method to numerically determine the dispersion relation when metallized interfaces are considered. Our data (see Fig. 9) are compared with previous experimental data given in [10, fig. 10], showing good agreement. We have simulated the structure there analyzed by means of the opened configuration drawn in Fig. 9. The perturbative nature of the elements of the BSDGF has been used to compute the integrals involved in the Galerkin method. A typical CPU time to generate one accurate value of the Galerkin determinant was about 1 s (seven trial functions like those in [16] were used).

V. Conclusions

At this point, it is important to emphasize some of the most relevant features of the EBM. We can enumerate them as follows:

- The EBM is essentially based on the uniqueness and equivalence electromagnetic theorems.
- It has been given a general algorithm to compute the BSGDF for any planar structure including any number of layers or metallized interfaces and any type of linear media.
- The complex general problem has been reduced to a chain of much simpler single-layered problems, which can be treated separately. These problems are solved by means of the mentioned matrix scheme, and the BSDGF is then built up by making use of the algebraic algorithms shown. By using this procedure we deal only with (2×2) matrices until that final inverse matrix of the BSDGF is formed.
- The EBM actually provides the $[\boldsymbol{L}]$ matrix, which is a block tridiagonal matrix. This fact simplifies the calculus if several metallized interfaces are involved.
- Important symmetry properties have been found to the involved matrices for many practical cases. This fact can make the determination of the BSDGF simpler.
- The EBM shows a proper numerical behavior on account of its perturbative nature.

The features and advantages mentioned above make the EBM a very powerful method to numerically determine the BSDGF.

Appendix

If the ith layer shows both dielectric and magnetic anisotropy, the characteristic tensor becomes

$$[\boldsymbol{M}]_i = \begin{bmatrix} \epsilon_{11} & \epsilon_{12} & \epsilon_{13} & 0 & 0 & 0 \\ \epsilon_{21} & \epsilon_{22} & \epsilon_{23} & 0 & 0 & 0 \\ \epsilon_{31} & \epsilon_{32} & \epsilon_{33} & 0 & 0 & 0 \\ 0 & 0 & 0 & \mu_{11} & \mu_{12} & \mu_{13} \\ 0 & 0 & 0 & \mu_{21} & \mu_{22} & \mu_{23} \\ 0 & 0 & 0 & \mu_{31} & \mu_{32} & \mu_{33} \end{bmatrix} \tag{A1}$$

and the (4×4) $[\boldsymbol{Q}]_i$ is, after all the algebraic manipulations,

$$\omega[\boldsymbol{Q}]_i = \begin{bmatrix} -k_x\bar{\epsilon}_{21} - k_z\bar{\mu}_{32} & -k_x\bar{\epsilon}_{23} + k_x\bar{\mu}_{32} & -\dfrac{k_xk_z}{\omega\epsilon_{22}} - \omega\mu_{31} + \omega\mu_{32}\bar{\mu}_{21} & \dfrac{k_x^2}{\omega\epsilon_{22}} - \omega\mu_{33} + \omega\mu_{32}\bar{\mu}_{23} \\ -k_z\bar{\epsilon}_{21} + k_z\bar{\mu}_{12} & -k_z\bar{\epsilon}_{23} - k_x\bar{\mu}_{12} & -\dfrac{k_z^2}{\omega\epsilon_{22}} + \omega\mu_{11} - \omega\mu_{12}\bar{\mu}_{21} & \dfrac{k_xk_z}{\omega\epsilon_{22}} - \omega\mu_{13} + \omega\mu_{12}\bar{\mu}_{23} \\ \dfrac{k_xk_z}{\omega\mu_{22}} + \omega\epsilon_{31} - \omega\epsilon_{32}\bar{\epsilon}_{21} & -\dfrac{k_x^2}{\omega\mu_{22}} + \omega\epsilon_{33} - \omega\epsilon_{32}\bar{\epsilon}_{23} & -k_x\bar{\mu}_{21} - k_z\bar{\epsilon}_{32} & -k_x\bar{\mu}_{23} - k_x\bar{\epsilon}_{32} \\ \dfrac{k_z^2}{\omega\mu_{22}} - \omega\epsilon_{11} + \omega\epsilon_{12}\bar{\epsilon}_{21} & -\dfrac{k_xk_z}{\omega\mu_{22}} - \omega\epsilon_{13} + \omega\epsilon_{12}\bar{\epsilon}_{23} & -k_z\bar{\mu}_{21} + k_z\bar{\epsilon}_{12} & -k_z\bar{\mu}_{23} - k_x\bar{\epsilon}_{12} \end{bmatrix} \tag{A2}$$

with $\bar{\epsilon}_{ij} = \epsilon_{ij}/\epsilon_{22}$ and $\bar{\mu}_{ij} = \mu_{ij}/\mu_{22}$.

REFERENCES

[1] R. Jansen, R. G. Arnold, and I. G. Eddison, "A comprehensive CAD approach to the design of MMIC's up to MM-wave frequencies," *IEEE Trans. Microwave Theory Tech.*, vol. 36, pp. 208–219, Feb. 1988.

[2] N. K. Das and D. M. Pozar, "Analysis and design of series-fed arrays of printed-dipoles proximity-coupled to a perpendicular microstripline," *IEEE Trans. Antennas Propagat.*, vol. 37, pp. 435–444, Apr. 1989.

[3] T. Itoh, "Spectral domain immitance approach for dispersion characteristics of generalized printed transmission lines," *IEEE Trans. Microwave Theory Tech.*, vol. MTT-28, pp. 733–736, July 1980.

[4] T. Kitazawa and Y. Hayashi, "Propagation characteristics of striplines with multilayered anisotropic media," *IEEE Trans. Microwave Theory Tech.*, vol. MTT-31, pp. 429–433, June 1983.

[5] A. Nakatani and N. G. Alexopoulos, "Toward a generalized algorithm for the modeling of the dispersive properties of integrated circuit structures on anisotropic substrates," *IEEE Trans. Microwave Theory Tech.*, vol. MTT-33, pp. 1436–1441, Dec. 1985.

[6] N. K. Das and D. M. Pozar, "A generalized spectral-domain Green's function for multilayer dielectric substrates with application to multilayer transmission lines," *IEEE Trans. Microwave Theory Tech.*, vol. MTT-35, pp. 326–335, Mar. 1987.

[7] W. C. Chew and L. Gurel, "Reflection and transmission operators for strips or disks embedded in homogeneous and layered media," *IEEE Trans. Microwave Theory Tech.*, vol. 36, pp. 1488–1497, Nov. 1988.

[8] L. Vegni, R. Cicchetti, and P. Capece, "Spectral Dyadic Green's function formulation for planar integrated structures," *IEEE Trans. Antennas Propagat.*, vol. 36, pp. 1057–1065, Aug. 1988.

[9] C. M. Krowne, "Fourier transformed matrix method of finding propagation characteristics of complex anisotropic layered media," *IEEE Trans. Microwave Theory Tech.*, vol. MTT-32, pp. 1617–1625, Dec. 1984.

[10] E. B. El-Sharawy and R. W. Jackson, "Coplanar waveguide and slot line on magnetic substrates: Analysis and experiment," *IEEE Trans. Microwave Theory Tech.*, vol. 36, pp. 1071–1078, June 1988.

[11] A. A. Mostafa, C. M. Krowne, and K. A. Zaki, "Numerical spectral matrix method for propagation in general layered media: Application to isotropic and anisotropic substrates," *IEEE Trans. Microwave Theory Tech.*, vol. MTT-35, pp. 1399–1407, Dec. 1987.

[12] R. Marques and M. Horno, "On the spectral dyadic Green's function for stratified linear media: Application to multilayered MIC lines with anisotropic substrates," *Proc. Inst. Elec. Eng.*, pt. H, vol. 134, pp. 241–248, June 1987.

[13] H. Lee and V. J. Tripathi, "Spectral domain analysis of frequency dependent propagation characteristics of planar structures on uniaxial medium," *IEEE Trans. Microwave Theory Tech.*, vol. MTT-30, pp. 1188–1192, Aug. 1982.

[14] S. C. Tsalamengas and N. K. Uzunoglu, "Radiation from a dipole in the proximity of a general anisotropic grounded layer," *IEEE Trans. Antennas Propagat.*, vol. AP-33, pp. 165–172, Feb. 1985.

[15] R. Marques and M. Horno, "Dyadic Green's function for microstrip-like transmission lines on a large class of anisotropic substrates," *Proc. Inst. Elec. Eng.*, pt. H, vol. 133, pp. 450–454, Dec. 1986.

[16] F. Medina, M. Horno, and H. Baudrand, "Generalized spectral analysis of planar lines on layered media including uniaxial and biaxial dielectric substrates," *IEEE Trans. Microwave Theory Tech.*, vol. 37, pp. 504–511, Mar. 1989.

[17] D. W. Berreman, "Optics in stratified and anisotropic media: 4×4 matrix formulation," *J. Opt. Soc. Amer.*, vol. 62, pp. 502–510, Apr. 1972.

[18] F. Medina and M. Horno, "Determination of Green's function matrix for multiconductor and anisotropic multidielectric planar transmission lines: A variational approach," *IEEE Trans. Theory Tech.*, vol. MTT-33, pp. 933–940, Oct. 1985.

[19] R. Boix and M. Horno, "Lumped capacitance and open end effects of striplike structures in multilayered and anisotropic substrates," *IEEE Trans. Microwave Theory Tech.*, vol. 37, pp. 1523–1527, Oct. 1989.

[20] M. Horno, F. Mesa, F. Medina, and R. Marques, "Quasi-TEM analysis of multilayered, multiconductor, coplanar structures with dielectric and magnetic anisotropy including losses," *IEEE Trans. Microwave Theory Tech.*, vol. 38, Aug. 1990.

[21] R. F. Harrington, *Time-Harmonic Electromagnetic Fields*. New York: McGraw-Hill, 1961.

[22] C. M. Krowne, "Electromagnetic theorems for complex anisotropic media," *IEEE Trans. Antennas Propagat.*, vol. AP-32, pp. 1224–1230, Nov. 1984.

[23] M. Kobayashi, "Reciprocity theorem for a region with inhomogeneous bianisotropic media and surface impedance," *IEEE Trans. Microwave Theory Tech.*, vol. MTT-24, pp. 114–116, Feb. 1976.

[24] M. Mrozowosky and J. Mazur, "Lower bound on the eigenvalues of the characteristic equation for an arbitrary multilayered gyromagnetic structure with perpendicular magnetization," *IEEE Trans. Microwave Theory Tech.*, vol. 37, pp. 640–643, Mar. 1989.

[25] D. M. Bolle, S. H. Talisa, "The edge-guided mode nonreciprocal phase shifter," *IEEE Trans. Microwave Theory Tech.*, vol. MTT-27, pp. 878–882, Nov. 1979.

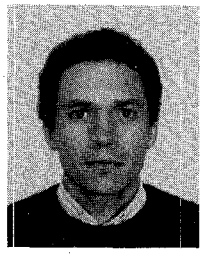

Francisco L. Mesa was born in Cádiz, Spain, in April 1965. He received the degree of Licenciado in physics in June 1989 from the University of Sevilla, Spain. He is currently in a Ph.D. program in microwaves with a scholarship from the Spanish Government. His research interests focus on planar lines on general anisotropic materials.

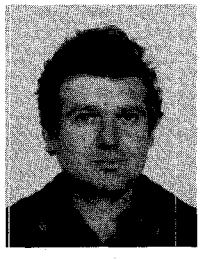

Ricardo Marqués was born in San Fernando, Cádiz, Spain. He received the degree of Licenciado in physics in June 1983 and the degree of doctor in physics in July 1987, both from the University of Sevilla.

Since January 1984, he has been with the Department of Electronics and Electromagnetism at the University of Sevilla, where he is currently Assistant Professor of Electricity and Magnetism. His main fields of interest include MIC devices design, wave propagation in anisotropic media, and electromagnetic theory.

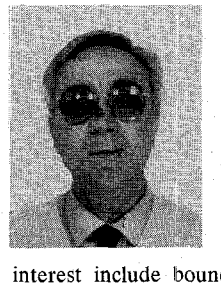

Manuel Horno (M'75) was born in Torre del Campo, Jaén, Spain. He received the degree of Licenciado in physics in June 1969 and the degree of Doctor en Ciencias in physics in January 1972, both from the University of Sevilla, Spain.

Since October 1969 he has been with the Department of Electricity and Electronics at the University of Sevilla, where he became an Assistant Professor in 1970, an Associate Professor in 1975, and Professor in 1986. His main fields of interest include boundary value problems in electromagnetic theory, wave propagation through anisotropic media, and microwave integrated circuits. He is presently engaged in the analysis of planar transmission lines embedded in anisotropic materials, multiconductor transmission lines, and planar slow-wave structures.